JOURNAL OF MATERIALS SCIENCE 37 (2002) 3261 – 3267

Architecture of thermal barrier coatings produced by electron beam-physical vapor deposition (EB-PVD)

JOGENDEN SINGH, DOUGLAS E. WOLFE
Applied Research Laboratory, The Pennsylvania State University, University Park, PA 16804, USA

JASON SINGH
Summer Student, State College High School, State College, PA 16801

Extremely high temperatures and severe atmospheric conditions in the hot section of aircraft engines during operation result in degradation and structural failures of turbine components. Replacing these components is very expensive. Thermal barrier coatings (TBC) composed of ZrO_2-8wt%Y_2O_3(8YSZ) applied by Electron Beam-Physical Vapor Deposition (EB-PVD) to turbine components offer excellent properties for thermal protection and resistance against oxidation - induced erosion and corrosion. However, the life of turbine components is still limited due to premature failure of the TBC. It is hypothesized that the life of the coated components can be extended by lowering the thermal conductivity of the TBC by creating multiple non-distinct or distinct interfaces and alloy additions such as Nb-oxide which will result in a reduction in the thermal conductivity and oxygen transport through the coating. This paper presents the microstructural results of standard 8YSZ, layered 8YSZ, Nb-oxide alloyed 8YSZ and functionally graded 8YSZ with Nb-oxide deposited by EB-PVD. TBC samples were examined by various methods including scanning electron microscopy (SEM), high-resolution optical microscopy (OM), X-ray diffraction (XRD), and thermal cycling tests. The preliminary results strongly suggest that multiple interfaced TBC exhibits better oxidation resistant properties as compared to standard and alloyed TBC.

1. Introduction

Turbine industry (auto, gas and steam) is continuously making efforts to increase the thermal efficiency of the engine as well as the life of the turbine components under severe environmental conditions such as wear, corrosion, and oxidation at elevated temperatures. Performance and life of turbine components is dependent on their operating temperature, with typical operating temperatures for aerospace turbine components of 1100–1200°C. As a result of excessive heat, an un-coated turbine component often cracks and corrodes. The life of turbine components is increased by applying oxidation resistant coatings composed of platinum-aluminide (Pt-Al) or MCrAlY alloys (M = Ni, Co, Fe, or mixed combination) followed by a thermal barrier coating (TBC). A typical TBC is composed of zirconium oxide with 8 wt% yttrium oxide (8YSZ), which is an ideal candidate for thermal protection coatings because of low density, low thermal conductivity, high melting point, and good thermal shock resistance, i.e., excellent erosion resistant properties. Typical physical properties of MCrAlY and 8YSZ are listed in Table I. TBC is generally applied by either the plasma spray or EB-PVD process with each having advantages and disadvantages. Generally, the life of a EB-PVD coating is superior to that of a plasma sprayed TBC as a result of the microstructural features inherent to the deposition process. Comparative properties of the 8YSZ coatings produced by plasma spray and EB-PVD processes are given in Table II. It should be noted that although the thermal conductivity of the 8YSZ deposited by plasma spray process is lower than 8YSZ deposited by EB-PVD, the thermal conductivity increases to the values of the EB-PVD 8YSZ within the first few hours of operation as a result of sintering. Table II shows that the EB-PVD TBC has almost a factor of 10 better adhesive strength which is important in preventing premature TBC spallation. In addition, the surface of the EB-PVD TBC is smoother, making it more attractive for aerodynamic reasons in the engine design.

In spite of significant advancements in coating processes, the life of coated turbine components is still limited under severe high temperature environmental oxidation and corrosion conditions. Premature coating spallation is often attributed to stress associated with the thermal expansion mismatch between the TBC and the bond coated substrate, as well as the continuous oxidation of the bond coat (often called thermally grown

TABLE I Physical properties of coatings

Materials	Linear CTE ($\times 10^{-6}$ K^{-1})	Thermal conductivity (W/m-K)	MP (°C)	Density (g/cm^3)	Elastic modulus (GPa)
YSZ	8.9–10.6	1 to 2.5 at 1100°C	2730	5.6	205
MCrAlY	15	85	1520	5.8	92

TABLE II Properties of 8YSZ coatings produced by EB-PVD and Plasma sprayed processes

Properties	EB-PVD	Plasma sprayed
Thermal conductivity (W/m-K)	1.5	0.8
Surface roughness (μm)	1.0	10.0
Adhesive strength (MPa)	400	20–40
Erosion rate (Normalized to EB-PVD)	1	7
TBC coating life in burner rig test (Normalized to EB-PVD)	5	1
Microstructure	Columnar	Lamellar

oxide-TGO). One of the approaches in reducing spallation of the TBC is to reduce the oxidation of the bond coating either by alloy additions or applying an additional coating layer which will reduce the oxidation of the bond coat. Strangman reported that the diffusion of oxygen was reduced by applying a 1 μm thick alumina (Al_2O_3) coating between the TBC and MCrAlY [1]. Alumina has very low oxygen diffusivity as compared with 8YSZ (10^{-19} and 10^{-11} m/s at 1000°C, respectively). In Strangman's work, the oxide layer was applied by chemical vapor deposition (CVD) process. Burner rig tests showed an increase in life of the coated pins from 15–35 hours to 95–143 hours at 1150°C (with 30 minute cycles). The increased life was attributed to the uniform dense Al_2O_3 coating applied prior to the TBC. Suppression of TGO formation is one of the current approaches being explored to minimize TBC spallation.

The second approach is to reduce the thermal conductivity of the TBC, which will result in a reduction in temperature that the base material and bond coat are exposed to, and thus the oxidation kinetics. In addition, a reduction in the oxygen transport mechanism through the TBC will provide an additional incentive in the suppression of TGO formation. Lower thermal conductive TBC is achievable by either developing new TBC with different compositions without sacrificing the physical and mechanical properties needed for the turbine industry and by modifying the microstructure and composition of the current 8YSZ.

An alternative TBC material having composition ZrO_2-25% CeO_2-2.5 wt%Y_2O_3 (YCSZ) is reported to have some benefits over 8YSZ including excellent phase stability at high temperatures and good corrosion resistant properties. However, results on the corrosion resistant properties of the YCSZ against vanadium attack are reported to be controversial [2]. Alloying 8YSZ with ceramic oxides such as CeO_2 or replacing Y_2O_3 by Sc_2O_3 including ZrO_2-20wt%Y_2O_3, ZrO_2-25% CeO_2 and ZrO_2-22% CeO_2-7 wt%Y_2O_3 reported to offer lower thermal conductivity, but also poor erosion resistant properties [3, 4]. Padture and Klemens recently reported a new TBC material composed of $Y_3Al_5O_{12}$ (YAG), whose conductivity is comparable to 8YSZ with relatively low oxygen diffusivity [5].

Recently, Dutton *et al.* [6, 7] investigated the thermal conductivity of multilayered coatings composed of Al_2O_3 and 8YSZ produced by plasma spray and EB-PVD processes. There was no reduction in thermal conductivity from either the reduction in individual layer spacing or by increasing the number of layers. It is necessary to point out that the thermal conductivity of Al_2O_3 (5.8 W/m-K) is about 5 to 6 times higher than 8YSZ (1–2 W/m-K). Thus, the net thermal conductivity of the composite coating, i.e., $Al_2O_3 + 8YSZ$ should be equal or higher than the EB-PVD 8YSZ, unless changes in the microstructure result in a reduction in the thermal conductivity. Dutton's work showed that the thermal conductivity was similar to a standard 8YSZ deposited by EB-PVD. It should also be noted that the microstructure of the EB-PVD multilayered coatings composed of $Al_2O_3 + 8YSZ$ were not columnar, which also suggests that the multilayer coatings were too dense (i.e., reduction in porosity), and thus an increase in the thermal conductivity. TBC with the columnar microstructure has many desirable properties including strain tolerance characteristics, which cannot be sacrificed at the expense of thermal conductivity.

The main objective of the present investigation was to modify the microstructure of 8YSZ applied by EB-PVD and reduce the oxygen transport by creating multiple interfaces. The second objective was to reduce the thermal conductivity of TBC by creating microporosity through alloying additions. It has been theoretically demonstrated that the thermal conductivity of ceramics can be controlled by graded porosity (microstructure refinement) and alloying additions without sacrificing other desirable properties [8–10]. To achieve this goal, it is important to understand the factors affecting the thermal conductivity of the materials which are summarized below.

Theory of conductance: The theory of thermal conductivity in solids is fully described in many places [11], and will only be briefly reviewed here. In crystalline solids, heat is transferred by three mechanisms: (i) electrons, (ii) lattice vibrations, and (iii) radiation. As zirconia and its alloys are electronic insulators, electrons play no part in conducting heat in these systems.

The contribution to thermal conductivity from lattice vibration (the quanta of which are known as phonons) is given by:

$$k_p = 1/3 C_v \rho v \lambda_p \quad (1)$$

where, k_p is the phonon thermal conductivity, C_v is the specific heat capacity at a constant volume, ρ is the material's density, v is the mean velocity of phonons in the material (speed of sound), and λ_p is the phonon mean free path.

Similarly, the contribution to the total thermal conductivity due to radiation is given by:

$$k_r = 16/3 B \eta^2 T^3 \lambda_r \quad (2)$$

where, η = refractive index of the material, B = Stephan-Boltzman constant, and λ_r = mean free

path of the radiation energy (i.e, photon mean free path). The total thermal conductivity of zirconia-based systems can then be described by the sum of these two terms:

$$k = k_p + k_r \quad (3)$$

Thus, to lower the thermal conductivity of the system, reduction in the specific heat capacity, phonon velocity and mean free path, density or refractive index (n) are needed. Specific heat capacity at constant volume for any system is constant above the Debye temperature (for zirconia, 25 J/K · mol) [11]. To engineer a lower thermal conductivity in the zirconia-based ceramics, the mean free paths of the heat carriers, their velocity, refractive index and the density of the material must be lowered.

In real crystal structures, scattering of phonons occurs when they interact with lattice imperfections. Such imperfections include vacancies, dislocations, grain boundaries, and atoms of different masses. The presence of impurity atoms and ions of differing ionic radius leads to increased anharmonicity and effects phonon scattering by locally distorting the bond length and thus introducing elastic strain fields into the lattice. The effects of such imperfections can be quantified through their influence on the phonon mean free path. This approach has been used by several researchers, for which the phonon mean free path (λ_p) is defined as:

$$1/\lambda_p = 1/\lambda_i + 1/\lambda_{vac} + 1/\lambda_{gb} + 1/\lambda_{strain} \quad (4)$$

where i, vac, gb represent intrinsic lattice structure, vacancy and grain boundary, respectively. Among these, the intrinsic lattice structure and strain field have the most significant effect on the phonon mean free path. The total mean free path of the phonon scattering can be reduced by alloying additions (i.e., solid-solution impurities), local strain fields and vacancies within the lattice. For the zirconia-based systems, workers in this field have demonstrated that increasing the level of yttria in the alloy has resulted in lower thermal conductivity due to the intrinsic mean free path decreasing with increasing yttria content [12–14].

In thermally sprayed TBC, typical grain size is of the order of 1–20 μm and grain boundaries are associated with inter-splat boundary porosity. In EB-PVD, TBC grain sizes vary from 1 to 2 μm at the interface, while the column length is 100–250 μm in the bulk of the coating. Keeping the total thickness of the TBC coating the same, the alignment of the inter-splat boundaries in the case of thermally sprayed coatings has a more pronounced effect than with EB-PVD, reducing the thermal conductivity of zirconia-yttria TBC materials from the theoretical values 2.2–2.6 W/m.K to values in the range 0.7–0.9 W/m.K (Table I). This behavior is well documented and is due to the reduction in mean free path of photons (radiative heat transfer) by scattering at the splat boundaries (i.e., inter-splat boundary porosity and grain boundary). This shows that the inter-splat porosity is more effective in reducing the thermal conductivity of the material than the columnar porosity in EB-PVD coatings. However, within the first few hours of operation, the thermal conductivity of plasma sprayed TBC increases due to sintering effects.

Typical microstructure of TBC produced by EB-PVD can be divided into two zones. The inner zone (I) is the early part of multiple nucleation and subsequent growth of the columnar microstructure having large number of interfaces, grain boundary and micro-porosity (Fig. 1). The thickness of the inner zone ranges from 5 to 10 μm and exhibits lower thermal conductivity (around 1.0 K/mK [15]). With increasing thickness, the structure is characterized by a dominant crystallographic texture and the thermal conductivity increases as the outer part of the coating becomes more perfect. In this outer zone (II), the thermal conductivity approaches that of the bulk zirconia (2.2 W/mK). Thus, modifying TBC structures should offer the best properties available from the commercial EB-PVD coatings and thermally sprayed ceramic coatings; namely, low conductivity, good strain tolerance, and good erosion resistance. Combination of layering at the micron level and introduction of density changes from layer to layer will significantly reduce the thermal conductivity of the coating (Fig. 1). As mentioned earlier, layer periodicity in the coating will significantly reduce both the phonon scattering and photon transport. The local changes in the density will contribute to phonon scattering and thus reduce the thermal conduction by the lattice.

The second approach to reduce the thermal conductivity of TBC is by alloying additions, i.e., uniform distribution of secondary phase particles within the matrix. The second element should have a different lattice parameter and thermal expansion co-efficient with respect

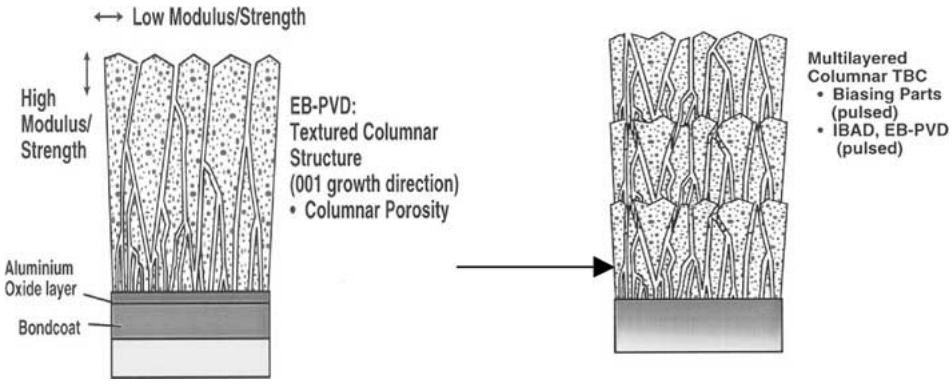

Figure 1 Schematic diagram showing modification of columnar microstructure into multi-layered porosity controlled columnar by ion beam assisted, EB-PVD.

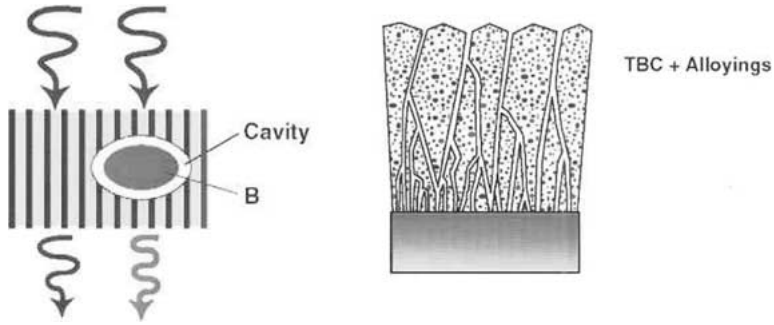

Figure 2 Schematic diagram showing the micro-cavity formation at the alloying addition (B) and matrix interface due to lattice mismatch.

to 8YSZ. During thermal cyclic exposure, micro-cracks will be formed around the secondary phase due to the stresses associated with the lattice mismatch. Fine distribution of micro-cracks will act like micro-porosity in the matrix and will reduce the thermal conductivity of the alloyed TBC as shown in Fig. 2.

2. Experimental procedure

Thermal barrier coatings were applied in an industrial prototype EB-PVD unit that has six electron-beam guns (Fig. 3) with each having a 45 kW average power capacity. The chamber will accommodate up to three ingots 7 cm in diameter and 50 cm long. The chamber is approximately 900 mm in length, 900 mm in width, and 900 mm in height. Physical vapor deposition (PVD) is primarily a line-of-sight process; therefore, uniform coating of complex parts, such as turbine blades, is accomplished by continuously rotating the turbine component during the coating process. The coating deposition rate and thickness depend on several parameters such as material being deposited, deposition time, chamber pressure, and operating power of the electron guns. For the alloyed TBC, two EB-guns were used to evaporate the coating materials (8YSZ and Niobium (Nb)) and two EB-guns were used to preheat the substrates indirectly by heating graphite plates. Coupons were mounted on a horizontal 2-inch diameter stainless steel shaft which was rotating above the melt pool at a speed of 7 revolutions per minute (rpm). The distance between the ingot melt pool and the coupons was ∼13 inches. During the evaporation of 8YSZ, external oxygen was injected into the vapor cloud to compensate the loss of oxygen and to maintain the desired stoichiometric composition of the TBC. Typical process parameters used for the present investigation are given in Table III.

TABLE III Typical process parameters used for evaporating 8YSZ ingots

EB-Voltage (kV)	18
EB-Current (Amp)	1.7
Substrate temperature (°C)	1000
Deposition time (hour)	1
Substrate rotation speed (rpm)	7

Four sets of experiments were performed (I-standard TBC, II-multilayered TBC, III-TBC + Nb-oxide as an alloying addition, and IV-8YSZ graded into 8YSZ + Nb-oxide and then graded back to 8YSZ). After measuring the samples, they were ultrasonically cleaned in acetone for twenty minutes, followed by rinsing with de-ionized water and then cleaned ultra-sonically with ethyl alcohol for ten minutes. Samples were again rinsed with de-ionized water and then dried with nitrogen gas. The samples were then tack welded separately onto a 1×1 inch stainless steel foil and again cleaned using the ultrasonic bath cleaner in the above-mentioned solutions. Samples were mounted on a mandrel for TBC deposition. Typical pressure inside the chamber during deposition process was about 1×10^{-3} Torr.

The standard 8YSZ was applied on the mounted coupons using the evaporation parameters as defined in Table III. The multilayered coating was formed by interrupting the continuous deposition of the TBC on the coupons, i.e., samples were periodically retracted from the vapor cloud during the deposition process. The alloyed TBC was produced by the co-evaporation of 8YSZ and Nb ingots. During the ingot evaporation process, external oxygen was injected into the vapor cloud at a flow of 100 sccm. Fractured surface and surface morphology of the coated samples were examined by a scanning electron microscope (SEM).

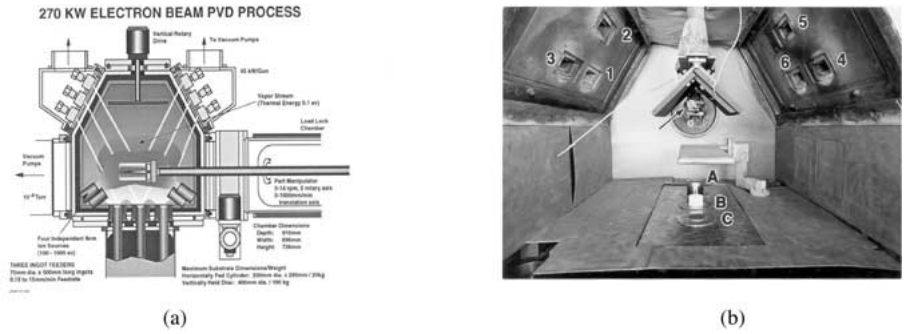

Figure 3 Electron Beam-Physical Vapor Deposition (EB-PVD) unit: (a) schematic diagram and (b) chamber photograph.

The cross-section of the coated samples was examined by optical microscope and electron microprobe. Phase analysis in the TBC coated samples was determined by X-ray diffraction.

3. Results and discussions

3.1. Microstructure of standard 8YSZ TBC

The coating thickness was found to be 165 μm with a total deposition time of 60 minutes. It was very difficult to differentiate the coating microstructure among the three type samples used in the present investigation. Since the microstructure of all the coated samples is comparable, only selective SEM micrographs are presented.

The typical microstructure of the TBC is shown in Fig. 4. The top view of the TBC shows uniformly faceted morphology with an average grain size of 5 μm. The fractured surface of the TBC coated samples reveals the side view of the columnar microstructure. At the TBC/ bondcoat interface, the size of the columnar grains was found to be relatively small (about <1 μm) and increased in size towards the tip of the column. All columnar grains were oriented in the same direction, i.e., perpendicular to the substrate. Inter-columnar and intra-columnar porosity was observed within the coating as shown in Fig. 4b and d, respectively.

3.2. Layered TBC

The layered structure was formed by removing the sample out of the vapor cloud every 10 minutes of deposition time for one minute (i.e., mounted samples were translated in and out of the vapor cloud 6 times during total deposition time of 66 minutes). It was anticipated that there would be a sharp interface at each interruption. The top view of all TBC-coated samples showed similar morphologies with differences in grain size observed as compared to Fig. 4. Microstructure appeared to have a faceted morphology, but with a smaller average grain size resulting from the interruption of coating condensation. Each grain shows preferred growth direction of the coating and porosity between the columnar grains. In order to see the sharp interface between the each interruption, a fracture surface was prepared as shown in Fig. 5c and d.

Fig. 5 clearly shows the six distinct 8YSZ layers. The total thickness of the coating was determined to be 165 μm with each layer thickness being approximately the same thickness (27 μm). The microstructure of the 8YSZ was found to be columnar with a "step like" image where the coating delaminated at the interfaces (Fig. 5c and d). It was difficult to get an average grain size of the coating because the size of the grains ranged from one to ten microns. The coating appeared very dense as compared to the standard 8YSZ (Fig. 4). This is believed to be directly related to the reduction in grain size and the creation of the distinct interfaces (nucleation and growth). Each interruption results in the TBC grains re-nucleating on the surface of the sample, thereby not allowing them to grow to the thickness of the coating.

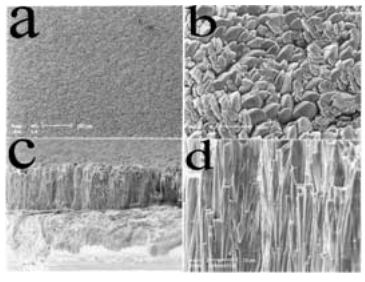

Figure 4 SEM micrograph of 8YSZ deposited on PtAl bond coated substrate showing (a) and (b) surface morphology and (c) and (d) fractured surface.

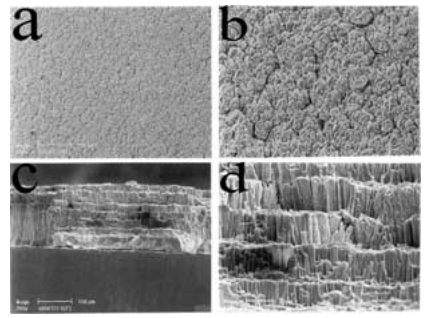

Figure 5 SEM micrograph of the layered 8YSZ TBC showing (a) and (b) surface morphology and (c) and (d) fractured surface with multiple interfaces.

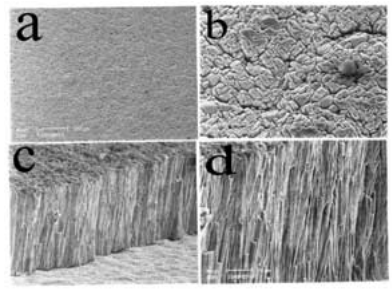

Figure 6 SEM micrograph of the Nb-alloyed 8YSZ TBC showing (a) and (b) surface morphology and (c) and (d) fractured surface.

3.3. Alloyed TBC with Nb-oxide

Both 8YSZ and Nb ingots were evaporated simultaneously to form an alloyed TBC, (i.e., TBC containing a fine dispersion of Nb in the form of an oxide). During the evaporation of both ingots, oxygen was injected into the vapor cloud to compensate the loss of oxygen and also to convert Nb into its oxide. All of the coated samples had a grayish color with no sign of coating delamination Fig. 6. The gray-ish color resulted from a deficiency of oxygen. Again, the average grain size ranged from one to ten microns. Coating morphology was comparable to standard TBC (Fig. 4).

3.4. Compositional graded TBC

The objective of the experiment was to form a compositional graded coating composed of 8YSZ layer followed by an alloyed TBC (i.e., 8YSZ + Nb-oxide) and again 8YSZ (Fig. 7). This compositional graded structure was achieved by the evaporation of standard TBC ingot for 10 minutes followed by co-evaporation of both TBC and Nb ingots for about 40 minutes and again only TBC ingot for 10 minutes. During the evaporation, oxygen was injected into the vapor cloud to compensate for the loss of oxygen and also to convert Nb into its

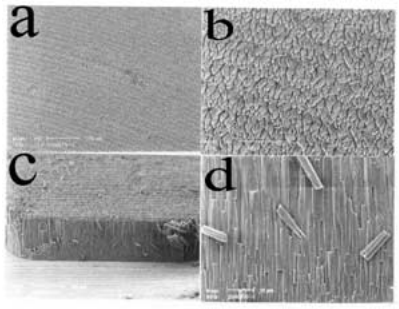

Figure 7 SEM micrograph of the TBC composed of 8YSZ / 8YSZ + Nb/ 8YSZ showing (a) and (b) surface morphology and (c) and (d) fractured surface.

oxide. The coating deposition was carried out sequentially and continuously without any interruption, therefore there was no sharp interface in the graded coating. Coated samples had a grayish color, again indicative of oxygen deficiency. The average grain size ranged from one to ten microns. The coating morphology was comparable with the standard and alloyed TBC (Figs 4 and 6, respectively).

4. X-ray diffraction of TBC

X-ray diffraction (XRD) patterns were obtained for coating conditions (I to III) as shown in Fig. 8a to c. Typical XRD pattern of the standard 8YSZ TBC showing the corresponding relative intensities of the various diffracted planes are shown in Fig. 8a. All the diffracted peaks from TBC have been identified as having a tetragonal phase. It is clear from Fig. 8a that the primary growth direction of the TBC is dominate along the ⟨200⟩ with maximum diffraction intensity 100%.

Slight differences were observed in the relative intensities of the diffracting planes in Fig. 8b. The differences in the relative intensities are a direct result of the degree of texturing. Using Fig. 8a as a standard 8YSZ diffraction pattern, the 8YSZ coating with the layered structure showed the largest deviation in relative intensities (Fig. 8b). This could be due to many factors including presence of a relatively large volume fraction of textured equiaxed grains in the layered structure. As each new layer of 8YSZ is formed, the grains nucleate on the previous 8YSZ layer. Initial grains will grow equally in all directions after which only those grains oriented in the preferred growth direction will continue to grow, resulting in columnar grains. Thus, this layered structure will be composed of textured grains with their dominant growth direction along the ⟨200⟩ as well as semi-textured grains. The size of the columns often varies in both length and diameter. Another factor that can result in changes in the relative intensities of the diffracting planes is the angle of columnar growth (i.e., angle of coating incidence). XRD of alloyed and the graded TBC (not shown) was similar to the standard TBC (Fig. 8a, c) as there was no change in the growth morphology of columnar grains. However, slight differences in the peak positions were observed as a result of strain associated with stress resulting from the compositional differences (i.e., addition of Nb) and the distinct interfaces.

5. Oxidation

Thermal stability of the TBC coatings and its effect on the oxidation rate of the bond coat were determined by exposing the coated buttons to 1175°C for 100 hours. Discoloration of the coated buttons was observed as shown in Fig. 9. The standard TBC coated button appeared to be relatively dark bluish color which is due to oxidation of bond coat and complete delamination (i.e., spallation) of TBC from the bond coated buttons (Fig. 9b). In contrast, the color of the layered TBC (Fig. 9c) coated button was still similar to that of the pre-exposed button (Fig. 9a). This indicates that the

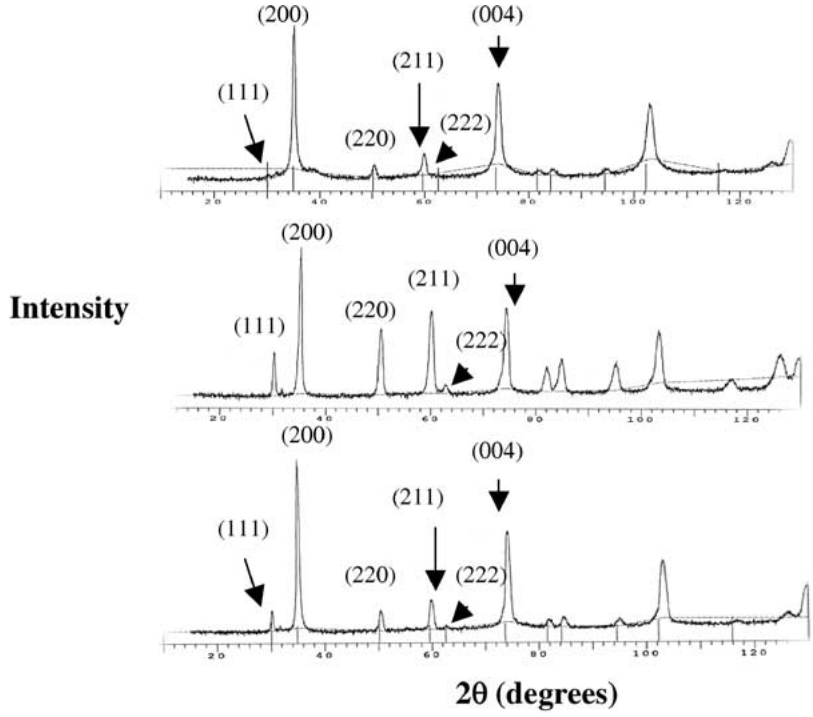

Figure 8 X-ray diffraction patterns of the TBC produced by EB-PVD for (a) I: standard 8YSZ, (b) II: layered 8YSZ, and (c) III: alloyed TBC (i.e., 8YSZ/8YSZ + Nb/8YSZ).

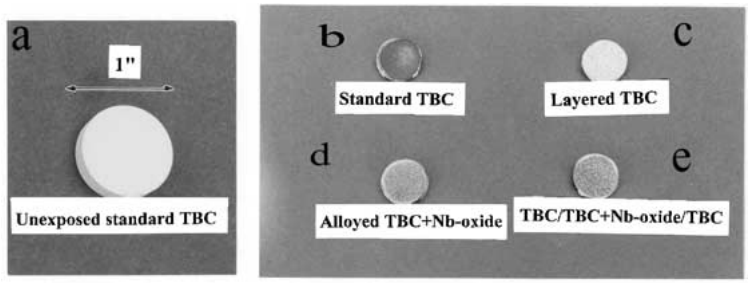

Figure 9 Photograph showing the oxidation of TBC coated buttons (a) unexposed standard 8YSZ and after thermal exposure at 1175°C for 100 hours for (b) standard 8YSZ coated button, (c) layered 8YSZ, (d) alloyed 8YSZ and (e) compositional graded TBC.

layered TBC coated button still has some coating with limited spallation and served as a oxidation barrier for the bond coat. The color of the alloyed and compositional graded TBC was relatively lighter bluish in comparison with the standard TBC (Fig. 9a, c and d). On comparing the color of the thermal exposed buttons, it is possible to comment that the layered TBC button exhibited better thermal protection in comparison with the alloyed TBC followed by the composition graded and the standard TBC. EDS analysis of the back side of the TBC coating revealed the presence of Co, Cr, Ni, Al, Zr, and O for Fig. 9b, d and e (elements present in both the bond coating and TBC). However, only Zr, Al and O were detected on the backside of the layered TBC (Fig. 9c). This strongly suggests that the layered structure reduced the amount of bond coating oxidation. However, further analysis needs to be performed to confirm these findings. Thermal cyclic tests including burner rig tests are still under way in understanding the oxidation rate and thermal stability of these coated samples.

6. Conclusion

The growth morphology of TBC structure was comparable for the standard 8YSZ, layered 8YSZ, and compositional graded 8YSZ TBC. In the layered TBC structure, new columnar grains nucleated and subsequently grew in each layer, and remained textured along ⟨200⟩ direction. Preliminary oxidation experiments showed that the layered TBC coatings exhibited better oxidation resistant properties as compared with the standard, alloyed and composition graded TBC.

References

1. T. STRANGMAN *et al*., U.S. Patent No. 4, 880, 614 (1989).
2. U. SCHULZ, K. FRITSCHER and M. PETERS, *Surface and Coating Technology* **82** (1996) 259.
3. U. SCHULZ, T. KRELL, U. LEUSHAKE and M. PETERS, in Proceedings of AGARD workshop on Thermal Barrier Coatings, Aalborg, DK, October 15–16, 1997.
4. M. MALONEY, in Thermal Barrier Coatings Workshop, Cincinnati, OH, 1997.
5. N. P. PADTURE and P. KLEMENS, *J. American Society* **80**(4) (1997) 1018.
6. K. RAVICHANDRAN, K. AN, R. E. DUTTON and S. L. SEMIATIN, *ibid.* **82** (1999) 673.
7. K. AN, K. RAVICHANDRAN, R. E. DUTTON and S. L. SEMIATIN, *ibid.* **82** (1999) 399.
8. P. G. KLEMENS and M. GELL, *Materials Science and Engineering* A **245** (1998) 143.
9. J. E. PARROTT and A. D. STUCKES, "Thermal Conductivity in solid" (Publ. Pion, 1975).
10. R. B. PETERSON, *Trans ASME J. Heat Transfer* **116** (1994) 815.
11. W. D. KINGERY, H. K. BOWEN and D. R. UHLMANN, "Introduction to Ceramics" 2nd edn. (John Wiley, New York, 1976) p. 617.
12. P. MORRELL and R. TAYLOR, *High Temperatures and High Pressures* **17** (1985) 79.
13. P. KLEMENS and M. GELL, in Proceeding of TBC Workshop, Cincinnati, OH, May 1997.
14. Y. A. TAMARIN, E. B. KACHANOV and S. ZHERZDEV, in 4th Int. Symp. Of High Temperature Corrosion, Les Embiez, France, May 1996.
15. J. R. NICHOLLS, K. J. LAWSON, D. S. RICKERBY and P. MORREL, in Proceedings of AGARD Structures and Materials Panel, Denmark, 1997, p. 6-1.

Received 24 April 2001
and accepted 25 February 2002